Dynamic views of ribosome function: Energy landscapes and ensembles

24

P. C. Whitford, R. B. Altman, P. Geggier, D. S. Terry, J. B. Munro, J. N. Onuchic, C. M. T. Spahn, K. Y. Sanbonmatsu, S. C. Blanchard

1. Introduction

Single-molecule fluorescence resonance energy transfer (smFRET) (reviewed in Munro et al., 2009) and cryo-electron microscopy (cryo-EM) investigations (Frank and Spahn, 2006; Spahn and Penczek, 2009; Fischer et al., 2010) of the translation apparatus reveal the ribosome's propensity to undergo large-scale fluctuations in conformation during function. Progress in these areas, building upon achievements in high-resolution structure determination of ribosomal subunits and functional complexes of the ribosome (Yusupov et al., 2001; Wekselman et al., 2009: Zhang et al., 2009; Gao et al., 2009; Demeshkina et al., 2010; Stanley et al., 2010), combined with an ever increasing breadth of computational modeling, simulation (Sanbonmatsu and Tung, 2007; Whitford et al., 2010a), and bioinformatics approaches (Roberts et al., 2008; Alexander et al., 2010), offers the potential to further broaden our understanding of the dynamic nature of the ribosome and translation components during protein synthesis. The large fluctuations observed by single-molecule studies, and the multitude of conformations reported by cryo-EM, make it clear that each „state" of the ribosome is in fact an ensemble of structurally similar configurations that are localized to a particular minimum on the free-energy landscape.

As single-molecule (Blanchard et al., 2004ab), cryo-EM (Frank and Spahn, 2006; Frank et al., 2007), rapid kinetics (Pape et al., 1999) and computational techniques (Sanbonmatsu et al., 2005) were first being extended to investigations of ribosome dynamics, the generally accepted goal was to identify specific "states" associated with biochemical steps in the translation process. This aim, driven by the canonical biochemical framework, held that structural and kinetic transitions in the ribosome were governed by factor- and GTP hydrolysis-driven transitions between a limited number of specific system configurations. However, the framing of the translation process in biochemical terms as a series of discrete "jumps" between distinct "states" mediated by specific translation factors often leads one to draw analogies between the ribosome and macroscopic machines which are inconsistent with both old and new observations in the field. First, the ribosome can synthesize protein in the absence of translation factors and nucleotide hydrolysis (Gavrilova et al., 1976), suggesting that translation is a function inherent to the ribosome. Second, as clearly demonstrated for other biopolymers (Frauenfelder et al., 1991), the ribosome is intrinsically dynamic. This aspect of ribosome function has now been highlighted by many recent smFRET measurements, wherein dynamics have been observed from a number of distinct structural perspectives. As evidence regarding the ribosome's intrinsically dynamic nature mounts (Dorner et al., 2006; Fei et al., 2008, 2009; Cornish et al., 2008, 2009; Munro et al., 2007, 2010a,b), it is increasingly apparent that the architecture of each translation component is designed to be inherently flexible and that further efforts must be made to describe function in this context.

An important consideration of dynamic systems is that even the lowest-energy "states" (*e. g.,* the classical state), are in fact large ensembles of physically distinct configurations. "States" are better defined as a set of configurations with similar free energies that rapidly interconvert, fluctuating around a local free energy minimum within a larger free energy landscape. In this view, the energy landscape of ribosome function is characterized by distinct free energy basins, each with a relative free energy minimum and free-energy barriers separating it from other basins. A deeper understanding of the ribosome's transit between

distinct basins on the free energy landscape during function is central to delineating key features of both elemental translation processes as well as the cellular strategies for translational control of gene expression. The free-energy landscape is an intrinsic property of a given molecular system, independent of the experimental/theoretical method employed to study it and various methodological approaches have emerged as a means to probe ribosome function from this perspective. These efforts are highlighted by advances in the area of time-resolved cryo-EM investigations of the translocation reaction coordinate (Fischer et al., 2010) as well as single-molecule fluorescence and theoretical investigations.

Single-molecule FRET measurements, as well as simulations, provide a powerful means of probing the properties of the free-energy landscape by providing information about the time spent within a given energy minimum before transitioning to another. While the insights obtained through such investigations portend a shift in our understanding of the translation mechanism, an apparent lack of consensus has emerged regarding specific dynamic events, in particular, the rates and amplitudes of motion and the number of intermediate configurations observed during global rearrangements in ribosome structure (Blanchard, 2009). In the context of highlighting early progress in monitoring ribosome activity at the single-molecule scale, this chapter attempts to define outstanding challenges facing the field and considerations that will be critical to delineating a quantitative framework for ribosome dynamics during function. Drawing from the protein folding community, a clear definition of the free-energy landscape of ribosome function is established, specific methods that can be used to measure features of the landscape are outlined, and the utility of the landscape view for understanding existing experimental data and protein synthesis regulation is explored. This template is provided to serve as a springboard towards next-generation experiments and a systems-level perspective on translation control.

2. Static states vs. ensembles of conformations

The first consideration to be made is that the term "state" implies the existence of a well-defined, deep, energetic minimum, where thermal fluctuations that may lead to structurally-similar configurations are insignificant. In this view, an exogenous source of energy, much greater than is available from the thermal bath, is necessary to mediate structural transitions in the system on a time scale necessary to support cellular translation. Recent smFRET and cryo-EM investigations of the pre-translocation complex provide evidence that distinct structural elements of the ribosome undergo spontaneous, transient transitions on a range of timescales (reviewed in Munro et al., 2009, 2010a,b). These data demonstrate the existence of metastable structural configurations of the ribosome stemming from reversible conformational events (subunit ratcheting/unratcheting; L1 stalk closure and opening; tRNA exchange between classical and hybrid configurations), whose relative populations depend on environmental variables and the ligands bound to the ribosome. Such observations suggest that the energetic barriers required to escape from each configuration of the system are small and the thermodynamic boundaries of each state are poorly defined. In this view, the number of identifiable "states" of the system depends on the probed degrees of freedom. Correspondingly, a substantially more comprehensive picture of the free-energy landscape underpinning ribosome function emerges where "states" are considered to be ensembles of structurally diverse configurations and thermal fluctuations are sufficient to promote substantial structural rearrangements. Moreover, if the free-energy landscape is not comprised of single, large barriers between distinct configurations, a variety of possible transition routes between "states" in the system may exist. Here, the total number of routes between local free-energy minima on the energy landscape can be collectively referred to as the transition state ensemble. As has been shown for protein structure-function relationships (Hyeon and Onuchic, 2007; Miyashita et al., 2003), the existence of structural heterogeneity within the ensemble suggests entropic contributions are critical to the architecture of the energy landscape, and correspondingly, ribosome function (Sievers et al., 2004; Whitford et al., 2010).

For the following discussions of energy landscapes, the differences between free energy, potential energy and enthalpy must be taken into consideration. The non-entropic component of the free energy can be referred to as enthalpy, effective enthalpy, or potential energy, depending on the context. A potential energy surface is distinct from the free-energy surface, as the latter also includes an entropic component.

A reduced description of the free-energy landscape of ribosome function is represented by the po-

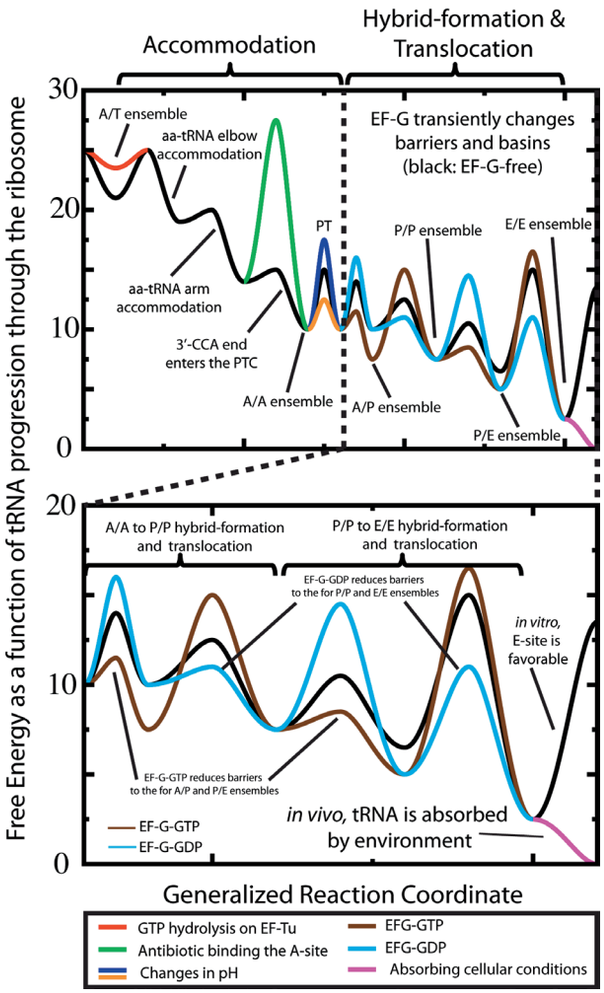

Fig. 1 Energy landscapes. Schematic representation of the potential of mean force (pmf) for a single tRNA molecule from the A/T configuration to when it leaves the E site. The black line represents the factor-free pmf. For simplicity, we discuss the pmf of a single tRNA molecule after averaging over the coordinates of the second tRNA. Perturbations to the landscape are schematized in color: (red) GTP hydrolysis by EF-Tu destabilizes the A/T ensemble; (green) antibiotic binding near the PTC could increase the barrier to aa-tRNA 3' CCA entry into the PTC since its displacement would be required for aa-tRNA accommodation; (blue/gold) changes in pH can alter the barrier/rate of peptidyl transfer (PT); (brown) EF-G-GTP can increase the rate of hybrid formation, and stability of the hybrid-state ensemble (i. e. lower barrier and lower minimum). (light blue) EF-G-GDP can increase the rate to, and stability of, the post-translocation ensemble. *In vivo* released E-site tRNAs are processed by cellular enzymes, making the chemical potential of spontaneous tRNA-binding energetically uphill (pink).

tential of mean force (*pmf*), the free energy of the system measured as a function of a particular coordinate. For instance, such a coordinate may describe movement of the tRNA through the ribosome, proceeding from the energy basin describing the A/T configuration of the ribosome to tRNA release from the E-site (Fig. 1). Here, the potential of mean force is given by $pmf(\vec{X}) = -k_B T \ln(P(\vec{X}))$, where $P(\vec{X})$ the probability of configuration $\vec{X}$ and k_B is Boltzmann's constant. In this schematic representation, the role of elongation factors can be depicted as transiently reducing the free-energy barriers associated with the transition state ensembles "ahead" of the tRNA molecule (in terms of movement of tRNA through the ribosome) and/or increasing the barriers associated with the transition state ensembles "behind" the tRNA. Similarly, the role of antibiotics can be represented as increasing the barriers associated with progression of the tRNA through the ribosome.

Quantitative descriptions of ribosome dynamics during translation are likely to emerge by applying the principles of energy landscape theory and the arsenal of quantitative tools largely developed in the protein and RNA folding fields (Bryngelson and Wolynes, 1989; Leopold et al., 1992; Onuchic and Wolynes, 1993; Onuchic et al., 2006; Wales, 2004; Onuchic et al., 2000; Thirumalai et al., 2010; Pincus, 2009; Thirumalai and Hyeon, 2005). This framework provides a uniform foundation for understanding the vast range of complex motions and energetic contributions associated with ribosome function. Understanding which features of the landscape are robust will be paramount in uncovering new mechanisms of control. If successful, this self-consistent, statistical physics-based framework may ultimately afford predictive control over ribosome function.

3. Choosing the energy landscape reaction coordinate

The first step in characterizing the energy landscape of any molecular process is to establish the proper reaction coordinate. A reaction coordinate is a measurable quantity that is uniquely defined for a given conformation. Since molecular systems possess 3N configurational degrees of freedom, where N is the number of atoms, projecting a given motion onto a particular reaction coordinate is often necessary to reduce the dimensionality of the dynamic process under investigation. Generally, an optimal choice of reaction coordinate will capture the barriers corresponding to the relevant kinetic steps of the system. This reaction coordinate should: (1) be continuous (*i. e.* local changes in structure are measured as local movements along the coordinate); (2) distinguish between starting and ending points of a transition and; (3) identify the tran-

sition state ensemble (TSE) (Nymeyer et al., 2000; Cho et al., 2006; Komatsuzaki et al., 2005; Das et al., 2006). An ideal reaction coordinate identifies the ensemble of conformations (the TSE) that are equally likely to reach the starting ensemble and the ending ensemble, where the TSE corresponds to the maximum in the *pmf* along a reaction coordinate.

While the system's free energy landscape determines its kinetic and thermodynamic properties, the *pmf* depends on the experimental observable. The difference between the underlying barrier and the measured barrier is apparent by considering the statistical mechanical definition of the probability for a given configuration:

$$P(\bar{X}) = \frac{\Lambda \exp\left(-V(\bar{X})/k_B T\right)}{Z}$$

where $\bar{X}$ is a 3N-dimensional vector describing the coordinates of the system, $V(\bar{X})$ is the potential energy at point $\bar{X}$, Z is the partition function of the system and Λ is the contribution to the partition function from the momenta integral. Here, the exponential in the numerator represents the velocity-independent, standard Boltzmann weight of a particular configuration. The denominator, Z, represents the unnormalized probability of all configurations. Thus, the pmf along any given reaction coordinate, Q, can be defined as,

$$pmf(Q) = \frac{\Lambda \int_V \delta\left(Q(\bar{X}) - Q\right) \exp\left(-V(\bar{X})/k_B T\right) dR^3}{Z}$$

where the observed *pmf*, *pmf(Q)*, will depend on its projection from 3N-dimensional coordinates onto the reaction coordinate, $(Q(\bar{X})$. This discussion is particularly relevant to smFRET experiments where changes in FRET efficiency as a function of time are used to monitor the reaction coordinate but are only typically monitored from a single structural perspective. Any single fluorophore labeling strategy can only produce one slice of the multidimensional energy landscape. Thus, distinct dye locations used to monitor a given conformational event may therefore lead to distinct conclusions regarding the system's dynamics. Such considerations provide a plausible explanation for why different labeling strategies for monitoring L1 stalk dynamics on the ribosome yield a different number of states (Fei et al., 2008; Cornish et al., 2009; Munro et al., 2010b) and how spontaneous ratcheting dynamics may be observed using one set of labeling strategies (Cornish et al., 2008, 2009), while using others they are not observed (Marshall et al., 2008). That is, each local minimum may be composed of an ensemble of configurations which is resolved by certain choices of dye locations and not by others. Specific reaction coordinates may mask or reveal more complicated features of the free-energy landscape (Garcia and Onuchic, 2003). The advent of technologies to monitor specific translation reactions from distinct structural perspectives (Cornish et al., 2008/9; Geggier et al., 2010) or multiple structural perspectives simultaneously (Munro et al., 2010a,b) can afford deeper insights into the relevant reaction coordinates of the process under observation. As additional technologies emerge to site-specifically position fluorophores in a greater number of positions within the translational apparatus, explicit control of the observed reaction coordinate can ultimately be obtained.

To provide a concrete example of how different reaction coordinates may lead to differential conclusions about the dynamics it is illustrative to examine a recently reported set of 312 independent all-atom simulations of tRNA accommodation (Whitford et al 2010). These data were used to calculate the probability distribution of the distance between the incoming aa-tRNA elbow and the P-site tRNA elbow (R_{Elbow}) as well as the distance between aminoacyl residues on A- and P-site tRNAs (R_3) (Fig. 2 A-D). The calculated probability distribution shows at least four highly populated ensembles accumulate during accommodation: the A/T ensemble, the elbow-accommodated ensemble, the elbow- and arm-accommodated ensemble, and the A/A ensemble. Along the (R_3) reaction coordinate (Fig. 2 B), there are several peaks that closely reflect the full distribution of states transited by the system (Fig. 2 A). In contrast, only two dominant peaks in the probability distribution are observed along the (R_{Elbow}) reaction coordinate (Fig. 2 C). These data show that both individual structural perspectives are limited and that only when the distribution is measured as a function of both (R_{Elbow}) and R_3 are the individual ensembles well separated.

Using a second reaction coordinate, the same simulations also revealed insights into the nature of L1 stalk motions. These data are of relevance to contextualizing recent smFRET studies of L1 protein motions in the pre-translocation complex (Munro et al., 2010a,b; Cornish et al., 2009; Fei et al., 2008). Here, the simulations showed large, thermally-accessible ($<6k_BT$) excursions in L1 stalk position as a function of time (Fig. 2E-H), where uncoupled twisting (±20 degrees) and extension (±20Å) motions of the L1 stalk occurred (Fig. 2F),

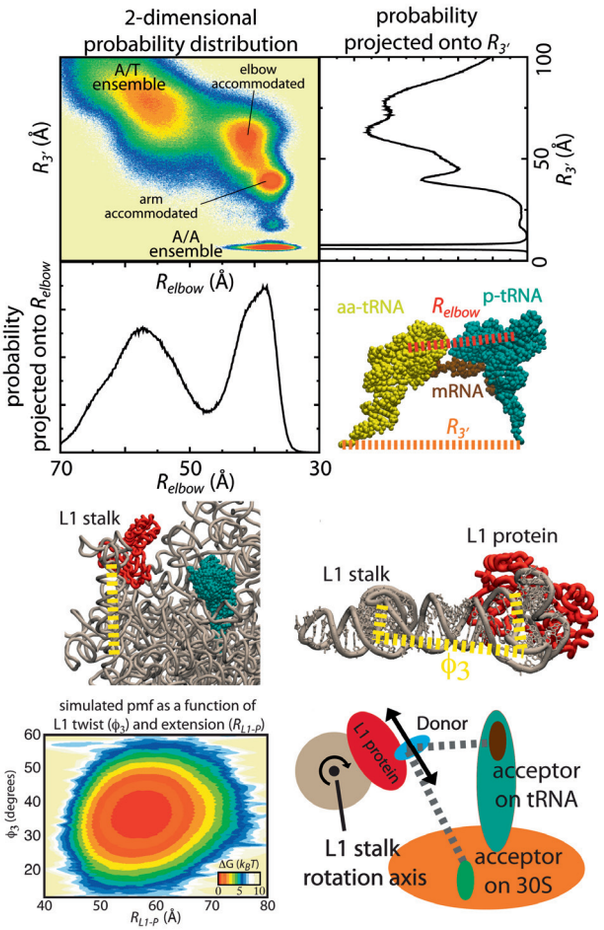

Fig. 2 Describing and using energy landscapes. (A) The probability of accommodation calculated from 312 independent all-atom simulations (Whitford et al 2010a) as a function of the distance between aa-tRNA and P-site tRNA elbows R_{Elbow} and amino acids $R_{3'}$. This distribution shows 4–6 peaks. (B) When the probability is calculated as a function of $R_{3'}$, not all peaks are clearly separated. (C) The probability distribution, as a function of R_{Elbow}, shows 2 dominant peaks. Some peaks in panel B are only present as shoulders in panel C. (D) Structural representation of R_{Elbow} and $R_{3'}$. (E) Structure of 23S rRNA (tan), P-site tRNA (cyan) and the L1 protein (red). (F) The L1 stalk "twist" coordinate, $\emptyset_3$, is defined by the pseudo-dihedral angle formed by the C1' atoms of G2127, A2171, C2196 & G2093 on the 23S rRNA. (G) The *pmf* as a function of the distance between the P-site tRNA and protein L1, $R_{L1\text{-}P}$, and $\emptyset_3$, calculated from all-atom simulations (Whitford et al 2010a), shows that large rearrangements in the L1 stalk (±20Å and ±20 degrees) occur with only a modest (few kBT) energetic penalty. (H) Schematic that illustrates how rotation of the L1 stalk is more easily detectable by smFRET if the donor and acceptor fluorophores fall along the tangent (double arrow) of the rotation.

which gave rise to a broadened ensemble of configurations (Fig. 2G). Such observations perhaps shed light on why a different number of states, with distinct rates of motion, were observed by the different groups using varied labeling strategies to measure L1 motion (Fig. 2H).

4. Further considerations in potential of mean force measurements

In addition to the aforementioned complexities associated with *pmf* measurement and calculation, it is also important to consider that the measured degrees of freedom in the smFRET measurement are in fact the distances between the transition dipoles of the fluorogenic centers, not the atoms to which they are attached. In most cases, the interdye distance can be approximated by their center of mass averaged over the imaging time interval. Anisotropic dye motions resulting from the steric contours of the molecule or site to which it is attached add a degree of uncertainty to this approximation. Rigorous comparison to the inter-atom and inter-dye distances also requires an estimation of how far the dyes extend away from the atoms to which they are attached.

As an example of the uncertainty in dye position in a smFRET experiment, fluctuations in inter-dye distance were calculated using all-atom simulations of the A/T ribosome configuration[1], where A- and P-site tRNAs were linked to Cy3 and Cy5 fluorophores, respectively, mirroring the labeling strategy used in smFRET imaging of aa-tRNA selection on the bacterial ribosome (Geggier et al., 2010) (Fig. 3A). A naive estimate of the barrier height to aa-tRNA movement from an A/T to A/A position based on the experimentally-derived probability distribution[2] suggests a barrier-crossing free energy of ~0.6 kT. Based on such an analysis, the elbow-accommodation time would be estimated to be ~1–10 ms, substantially faster than anticipated from bulk kinetics (Rodnina and Wintermeyer, 2001; Johansson et al., 2008), previous smFRET experiments (Blanchard et al., 2004; Lee et al., 2007) as well as hidden-Markov modeling (Geggier et al., 2010). Here, a simple numerical exercise provides important insights into how functionally relevant barrier

1 This near-A/T model was obtained by using a flexible-fitting algorithm (Orzechowski and Tama, 2008), in conjunction with a structure-based forcefield (Whitford et al 2009a, 2009b) and an unpublished cryo-EM map, as implemented elsewhere (Ratje et al., 2010).

2 This naive estimate was not reported in previous publications. Here, we simply used the logarithm of the probabilities obtained in the previous study to illustrate how the barrier height is likely underestimated by this approach.

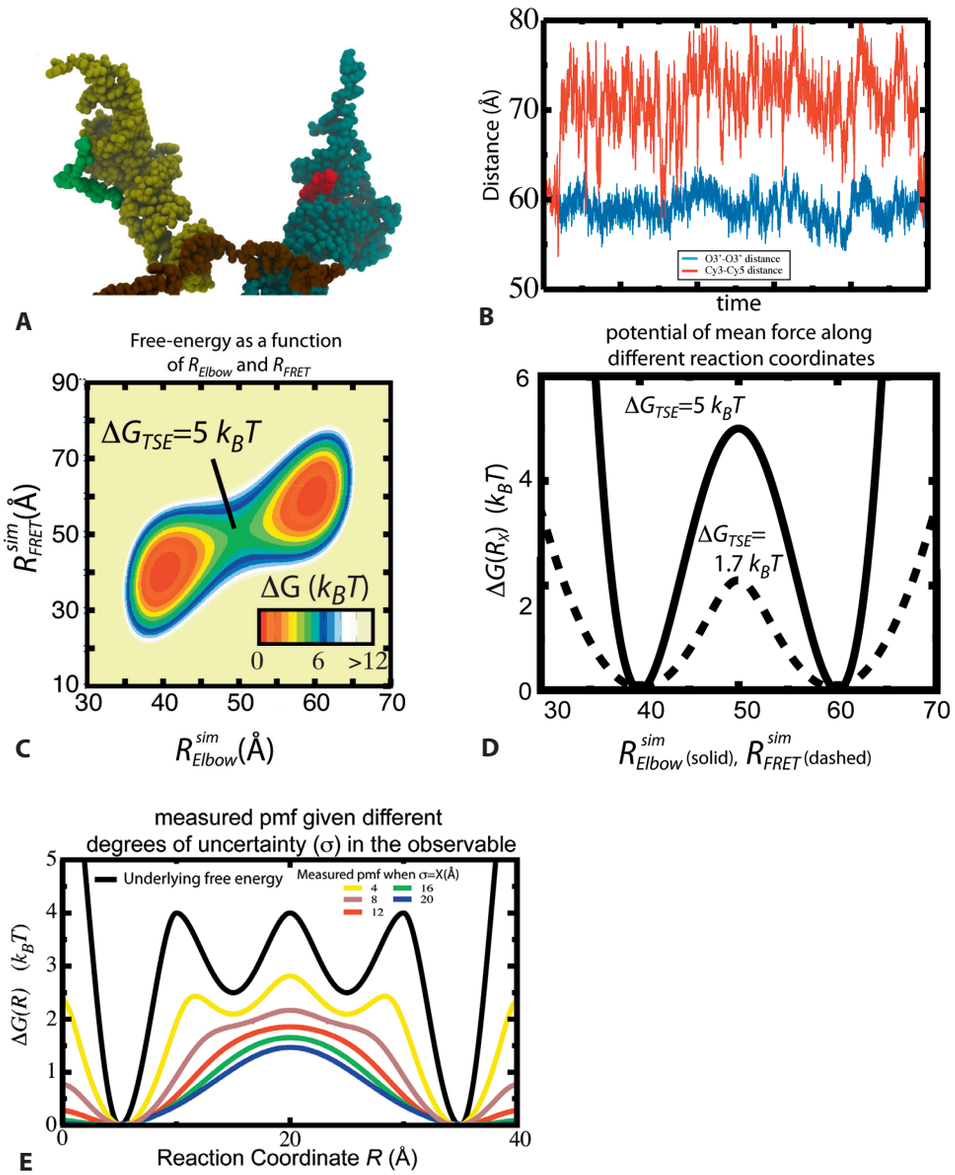

Fig. 3 Fluctuations in FRET dye position can alter the measured pmf. (A) Structural representation of aa-tRNA (left, yellow), P-site tRNA (right, cyan), mRNA (brown), Cy3 dye (green) and Cy5 dye (red). (B) Distance between the center of Cy3 and Cy5 (red) and R_{Elbow} as functions of time for an all-atom simulation of a near-A/T conformation. Fluctuations in R_{Elbow} are ~ 3 Å and fluctuations in dye distance is ~10 Å. (C) Hypothetical free-energy profile, with dispersion in dye distance of ~12 Å and a free-energy barrier of 5 Å. (D) Free energy in panel C projected onto the dye distance (dashed line) shows a barrier of ~ 1.7 kBT. When projected onto R_{Elbow} (solid line) the barrier is 5 kBT. The pmf along the dye distance will likely underestimate the free-energy barrier. (E) Uncertainty in the projection onto a reaction coordinate can mask barriers in the landscape. A potential free-energy profile is shown in (black). As done in panel C, this profile is described by a two-dimensional landscape, where the uncertainty in the observable (sigma, σ) is given a particular width and the "observed" pmf is then calculated. As sigma is increased, the intermediate minima are less pronounced.

heights can be difficult to estimate from FRET probability distributions projected along the experimentally-obtained tRNA-elbow distance (Fig. 3).

When the free-energy barrier associated with a transition exceeds several k_BT, where barrier crossing events occur infrequently, then over reasonably long time intervals (ca. milliseconds) the time-averaged center of mass position of the Cy3 and Cy5 fluorophores provides a close approximation of the average tRNA position. In this regime, the Cy3 and Cy5 fluorophores tumble rapidly relative to the rates of large-scale tRNA motions and large changes in distance between the center of mass of the Cy3 and Cy5 fluorophores occur only during barrier-crossing events. However, when imaging time scales approach the rates of Brownian fluctuations in fluorophore position (e. g., microseconds), then the inter-dye distance fluctuates significantly even in the absence of appreciable changes in the A- and P-site tRNA inter-elbow distance. In this regime, dye mobility contributes significantly to the experimentally measured *pmf*. Simulations suggest that dye positions may vary by as much as 12 Å on the nanosecond-microsecond time scale. To illustrate this point, the *pmf* of the A/T to A/A transition for both, R^{sim}_{Elbow} and R^{sim}_{FRET} probability distributions can be projected onto the reaction coordinates and analyzed according to statistical mechanics[3]:

$$\Delta G\left(R^{sim}_{FRET}\right) = -k_B T \ln\left(P\left(R^{sim}_{FRET}\right)\right)$$

This analysis shows that the estimated barrier height for motion based on R^{sim}_{FRET} (1.7 kBT) is substantially lower than for R^{sim}_{Elbow} (5 kBT), which is due to both experimental noise[4] and uncertainties in dye position (Fig. 3D). As the rate of barrier-crossing is proportional to $e^{-\Delta G_{TSE}/k_BT}$, where ΔG_{TSE} is the barrier height and TSE is the transition state ensemble, such differences correspond to about a factor of 30 in timescale. Thus, broadening of the observed probability distribution due to the ratio of signal-to-noise and dye mobility considerations in smFRET measurements tend to provide underestimates of the physical barrier height and therefore overestimate the rates of motion. As the uncertainty in the observable increases, the likelihood of observing subtle features of the underlying energy landscape diminishes (Fig. 3E). At the same time, fast conformational events can be missed in smFRET measurements (Blanchard et al 2004a), having the opposite effect of providing estimates of the rates of motion that are slower than reflected by the true barrier heights. As the uncertainty in the projection onto a reaction coordinate changes, or if different reaction coordinates are employed, the measured pmf will be systematically altered.

Such considerations represent important challenges for all single-molecule fields. An important avenue by which to explore these issues is to simulate "noise-less" smFRET data according to explicit kinetic models of motion and then to simulate different types and amplitudes of noise to enable direct comparisons to the experimental data (Munro et al., 2007; Geggier et al., 2010). Progress may also be made by delineating methods for choosing the ideal reaction coordinate for a given transition. Such pursuits may be aided by (i) computational/theoretical efforts (Faradjian and Elber, 2004; Peng et al., 2010; Das et al., 2006) and (ii) more rigorous approaches for understanding the nature of fluorophore mobility in their biological contexts. While, in principle, it should be possible to choose an optimal reaction coordinate, performing experiments and simulations with probes in different positions may ultimately be necessary to provide the quantitative information necessary to determine robust features of the underlying energy landscape of a given conformational transition.

5. The role of diffusion in energy landscapes: connecting kinetics and thermodynamics

While no direct experimental measurements have been aimed at determining barrier-crossing attempt frequencies in the context of the translation apparatus, recent smFRET measurements of aa-tRNA selection (Geggier et al., 2010) and pre-translocation complex dynamics (Munro et al., 2010a,b) have observed what can be considered "non-productive" transition attempts to achieve key intermediate configurations during the process of aa-tRNA selection and translocation, respectively. During selection, aa-tRNA was described as sampling "GTPase-activated" and "accommodated" configurations prior to undergoing the chemical steps of GTP hydrolysis and peptide bond formation, respectively. The pre-translocation complex was shown

3 Since the surface in Fig. 2C is defined as a function of R^{sim}_{FRET} and R^{sim}_{Elbow}, "projecting" onto R^{sim}_{FRET} simply means calculating the appropriate sum over R^{sim}_{Elbow} for each value of R^{sim}_{FRET}.

4 In this discussion we are focusing on the contribution of dye uncertainty. Though, currently, additional sources of noise are likely comparable in scale.

to transiently achieve a FRET configuration consistent with formation of the unlocked state, the putative intermediate for translocation. Such notions of non-productive conformations, which bear resemblance to the transition states of barrier crossing, are consistent with the stochastic nature of barrier-crossing processes. The following general relationship describing diffusive motions in molecular systems provides an important bridge between the free-energy landscape and the kinetic parameters of ribosome function (Bryngelson and Wolynes, 1989; Zwanzig, 1988):

$$\frac{1}{k} = \langle \tau \rangle = \int_{R_{start}}^{R_{end}} dQ \int_{\infty}^{R} dQ' \frac{\exp\left[\left(G(Q) - G(Q')\right)/k_B T\right]}{D}, \quad (1)$$

where k is the rate of barrier crossing, <τ> is the mean-first passage time, *Q* is the reaction coordinate, *D* is the effective diffusion coefficient in reaction-coordinate space, and Rstart and Rend are the endpoints of the transition. The diffusion coefficient *D* is often assumed constant and particle diffusion in three dimensions can be estimated according to the Stokes-Einstein relationship, $D = k_B T / 6\pi\eta\alpha$, where η is the viscosity of water and *a* is the hydrodynamic radius. Through analysis of kinetic models and experimental data, Fluitt et al. (2007) estimated the diffusion coefficient of ternary complex in solution to be ~2.6 mm^2/s. As the hydrodynamic radius of ternary complex is roughly two-fold larger than the tRNA molecule, tRNA diffusion in solution can be estimated to be ~5.2 mm^2/s. Scaling by an additional factor of one-third to account for the approximately 1-dimensional diffusion of tRNA as it moves through the ribosome (i. e. along the R_{Elbow} vector) reduces this value to 1.7 mm2/s, in good agreement with explicit-solvent simulations of the 70S ribosome (205–301 ns each), estimating the diffusion in R_{Elbow} to be ~ 1 mm^2/s (Whitford et al., 2010b). Advances in experimental and computational methods (Nettels et al., 2008; Wong and Case, 2008) may allow for more precise estimates of the diffusive properties of tRNA inside the ribosome, though such studies have not been reported to date. Full characterization of the diffusive properties will allow for a quantitative relationship between kinetics and thermodynamics, as well as for direct comparisons to rates determined in bulk (Gromadski and Rodnina, 2004) and single-molecule methods. However, for sufficiently large energy barriers, the rate of barrier crossing (equation 1), can be simplified through the introduction of a prefactor, C, that approximates the diffusive properties, manifested as a barrier-crossing attempt frequency:

$$\frac{1}{k} = \langle \tau \rangle = \frac{1}{C} \exp\left(\Delta G_{TSE} / k_B T\right), \quad (2)$$

One can think of the prefactor as describing how frequently the barrier crossing events are attempted, where the probability of successful crossing is determined by the barrier height. Investigations of the folding properties of small proteins suggest that C is ~0.1–20 μs^{-1} (Kubelka et al., 2004; Tang et al., 2009). Thirumalai and Hyeon (2005) similarly estimate *C* for RNA folding to be ~1 μs^{-1}. Explicit-solvent simulations of the 70S ribosome also suggest the prefactor associated with tRNA elbow-accommodation to be ~ 1 μs^{-1} (Whitford et al., 2010b). Here, it is important to note that a sharp distinction should be made between the prefactor associated with conformational rearrangements and the prefactor associated with the transition state for catalysis. Classical biochemical transition-state theory was developed in the context of enzyme catalysis, where the attempt frequency to the chemical transition state is governed by covalent bond stretching and bond angle bending. Since these vibrations occur on femtosecond to picosecond timescales, the attempt frequencies should occur in a similar time domain. However, in the case of conformational rearrangements where the attempt frequency is limited by multi-dimensional diffusion on the energy landscape, barrier-crossing attempts will be far more rare and dependent on the functionally-relevant degrees of freedom in the system. The observation of "non-productive" sampling events on path to productive aa-tRNA selection and translocation suggests that barrier-crossing attempts may be observed in both the microsecond and millisecond regimes. As the time-resolution of smFRET imaging experiments continues to increase, intermediates of this nature are likely to be more frequently detected and more critical to mechanistic discussions of ribosome function.

6. Energetic coupling between ribosomal compo nents

While the notion that the ribosome acts as a "thermal ratchet" (Spirin 2009) implies that the energetic barriers of large-scale ribosomal subunit motions are small relative to thermal fluctuations, it has only recently been suggested that th is may be the case

throughout the translation cycle (Munro et al., 2009). Analogous to protein folding landscapes (Onuchic et al., 2000), broad energetic basins separated by lower barriers ensure physiologically-relevant timescales of function. Such a landscape is consistent with a scenario where many independent, thermally-accessible motions within the ribosome may be anticipated to occur, and whose timescales are dependent on the diffusive properties of the system. Experimental observations of independent degrees of freedom in the pre-translocation complex that appear loosely coupled support this notion (Munro et al., 2010a, b).

Formally, coupled degrees of freedom represent conformational events that are structurally distinct, but not energetically separable. A general expression of the total potential energy of a system, V, and the coupling between conformational events can be given by the equation:

$$V = W_U(V_1(R_1) + V_2(R_2)) + W_C V_C(R_1 R_2), \quad (3)$$

where $V_i(R_i)$ is the separable contribution to the potential due to degree of freedom R_1, $V_C(R_1,R_2)$ is the inseparable contribution due to coupling between the R_1 and R_2, W_U is the scale of the uncoupled contribution and W_C is the scale of the coupling interaction. Assuming entropy is constant as a function of R_1 and R_2, the free energy of the system reduces to the potential energy. One can define the degree of coupling in the system, Γ, as the ratio of the coupled and uncoupled contributions, W_C/W_U. In the limit of uncoupled motions, $\Gamma \sim 0$. For weakly coupled systems, $\Gamma << 1$. When the contribution of the coupled and uncoupled terms are comparable, corresponding to a moderately, or loosely, coupled system, $\Gamma \sim 1$. When $\Gamma >> 1$, the coupled interactions dominate the dynamics and the system should be considered strongly coupled. Fig. 4A-C illustrate how the energy landscape of a conformational process involving two structurally distinct degrees of freedom may change as Gis increased. In the uncoupled case, each degree of freedom is independent, and there are two intermediate ensembles between the two endpoints (the upper-right and lower-left basins are considered the "endpoints"). At $\Gamma = 0.8$ the two intermediate ensembles become less populated, and it is more likely the system will move along both coordinates simultaneously. For $\Gamma = 6$ the two intermediates become highly destabilized and only two basins in the free energy landscape, the starting and ending configuration, are populated.

Relating such landscapes to experimental observables, trajectories of diffusive motion similar to those that may be obtained from a single-molecule measurement may be generated via Brownian dynamics simulations where the movement across the landscape of a "pseudo-particle" evolves in time (Fig. 4D-F). From such trajectories, the autocorrelation and cross-correlation functions of the variables can be calculated (Fig. 4G-I). Here, both the distance trajectories (Fig. 4D-F) and the correlation data (Fig. 4G-I) reveal that movements along the two reaction coordinates are indeed independent for $\Gamma = 0$ and increasingly coupled as G increases. This illustrative example suggests that a reasonable experimental measure of the degree of coupling, Γ_{corr}, of a given process may be estimated by the ratio of the decay times for the cross-correlation function (τ_{cross}) and the autocorrelation function (τ_{auto}). When the degrees of freedom are uncoupled, τ_{cross} and Γ_{corr} are both zero. As coupling increases, τ_{cross} and τ_{auto} become comparable, and Γ_{corr} approaches 1. With continued advances in multi-color smFRET technologies, where multiple degrees of freedom can be probed simultaneously (Munro et al 2010b), quantitative measures of the degree of coupling between any two degrees of freedom may be possible.

7. Energy landscapes and X-ray crystallography

At first glance, these dynamic views of ribosome function may appear at odds with the static structures obtained using x-ray crystallography and cryo-EM methods. However, if these two experimental approaches are considered in terms of the associated energy landscapes during data collection, the results of such studies are indeed consistent with the ensemble description provided through single-molecule methods.

For context, this discussion will focus on the process of cognate aa-tRNA accommodation, for which both structural (Villa et al., 2009; Schuette et al., 2009; Schmeing et al., 2009) and functional (Gromadski et al., 2004; Geggier et al., 2010) information have been recently obtained. Fig. 5A shows a simplified schematic of a possible energy landscape for tRNA accommodation as it may occur in solution (black line).[5] In this con-

5 It should be noted that this schematic is not intended to be all-inclusive. That is, the landscape may possess substantially more detail (Geggier et al 2010), though for demonstrative purposes we used this overly-simplified representation.

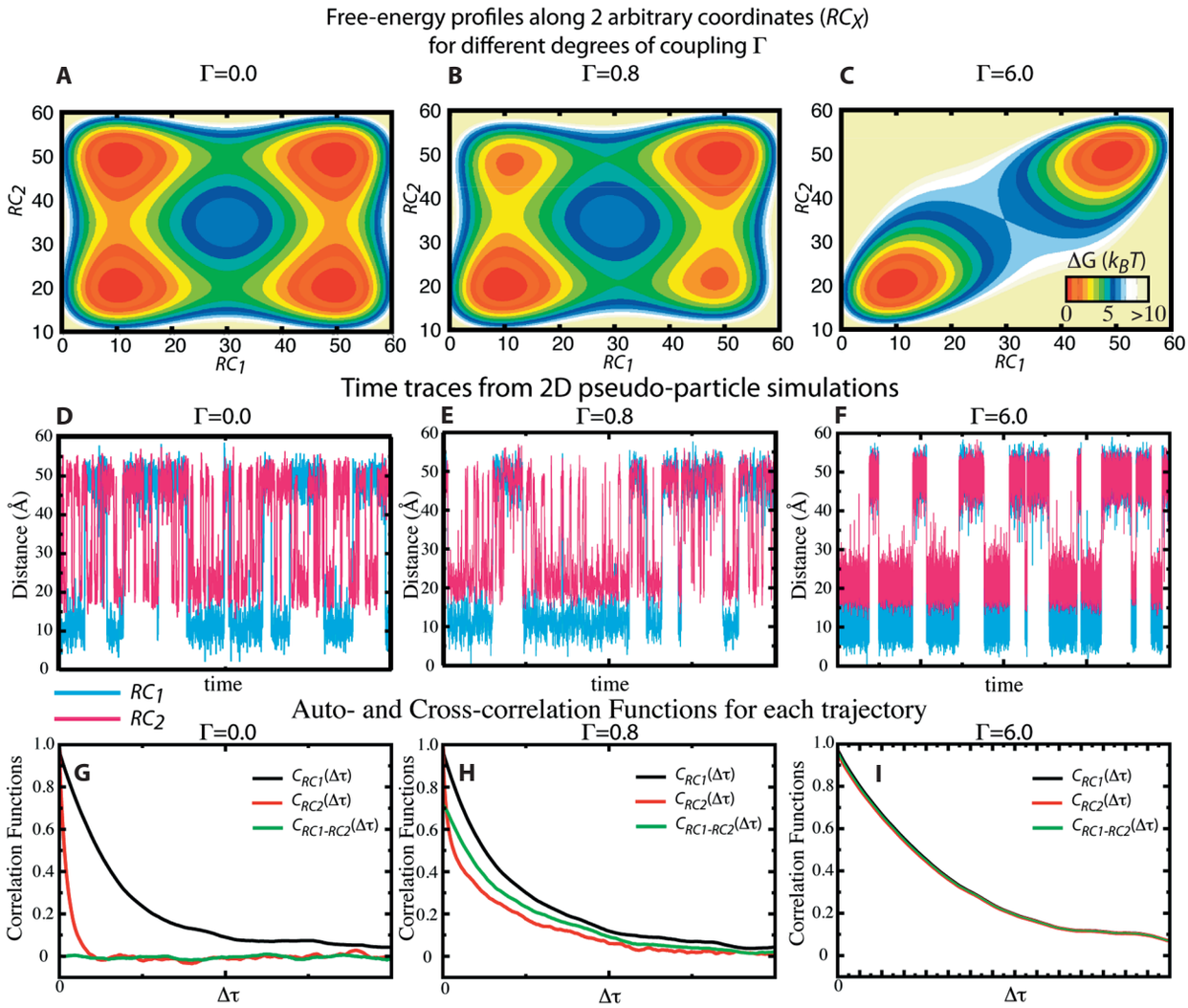

Fig. 4. Energy landscapes provide intuitive measures of coupling between coordinates. **(A-C)** Three energy landscapes with varied degrees of energetic coupling between the two reaction coordinates (Γ=0, 0.8 and 6). Each landscape is represented as the sum of two independent contributions to the landscape (one for each coordinate), each with two minima, plus an interaction term that harmonically couples the two coordinates (see main text). In **(A)**, the coordinates are uncoupled (Γ=0), and the free-energy basins indicate it is equally likely to populate any combination of end states. That is, the free energy of the four basins is the same. Simulating diffusive motion of a "pseudo-particle" on this landscape **(D)** shows that movement along the two coordinates is independent, as verified by the near-zero cross-correlation function (G; labelled $C_{RC1\text{-}RC2}$). When the energetic contribution of the coupling term is comparable (i. e. loosely coupled) to that of the uncoupled term (B) the intermediate basins are destabilized, (E) there is a visible correlation between the coordinates and (H) the timescale of decay of the cross correlation function approaches that of the autocorrelation functions for each coordinate (C_{RC1} and C_{RC2}). In the tightly-coupled case (C) there are no longer any independent intermediate basins, the time traces of the coordinates (F) are visibly closely related and the cross- and auto-correlation functions are indistinguishable. While Γ provides a quantitative measure of the degree of coupling, in terms of energy, cross-correlation functions from multi-color smFRET provide an experimental measure of coupling.

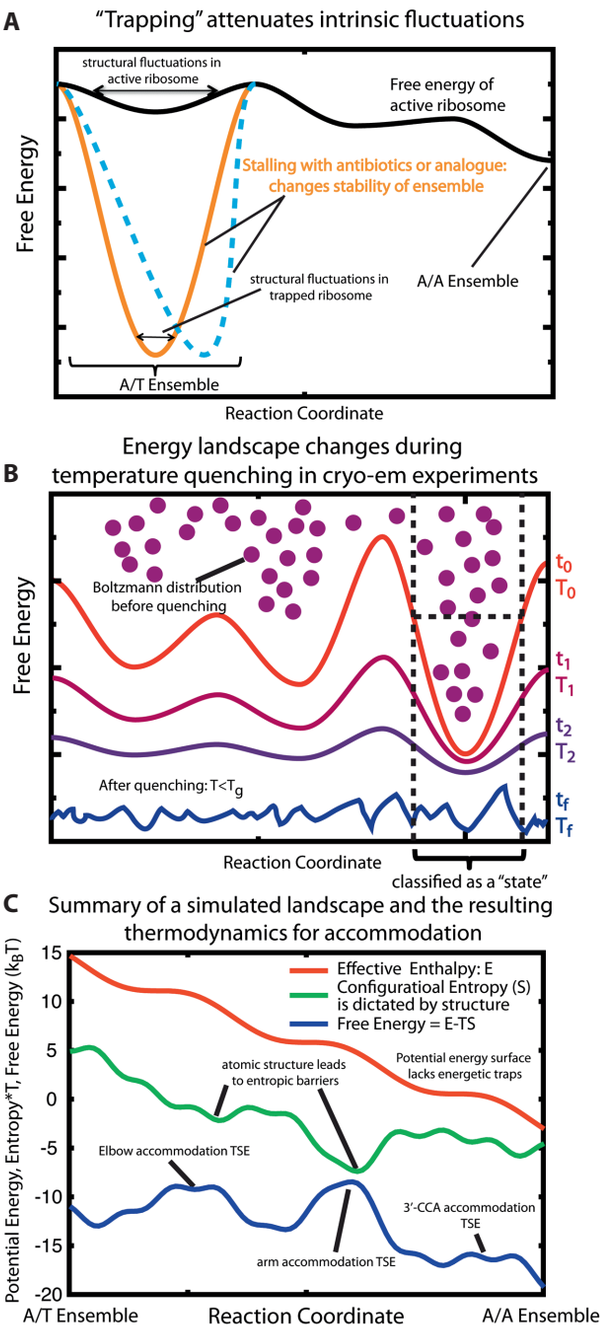

Fig. 5. Energy landscapes in crystals, cryo-EM, and simulations. (A) When determining a crystal structure, it is necessary to "trap" the conformation. Energetically, this is represented as a significant decrease in the free energy of a particular ensemble (gold or dashed blue). Since the basin is not (infinitely deep and sharp, thermal fluctuations will lead to finite degrees of motion (arrows) inside the crystal. Certain fluctuations will be attenuated by lattice contacts between adjacent ribosomes in the crystal, and the energetic basin may shift (dashed blue). For example, because the L1 and L11 stalks are likely flexible (i. e. small energetic perturbations can significantly shift the distribution of configurations), the stalk ensembles will be affected by such interactions. (B) In a cryo-EM experiment, the pre-quenched ensemble follows a Boltzmann distribution. During quenching, if the glass transition temperature is reached ($T < T_g$) faster than the reconfiguration time of the system, the final frozen ensemble will be a Boltzmann distribution at the original temperature (T_X is the temperature at subsequent points in time t_X after quenching is initiated, $t_X < t_{X+1}$). During data analysis, maximum-likelihood methods are used to identify "states". Future work should determine what a "classified state" is energetically. (C) Functional forms of the energy landscape may be tested through simulation. When using an energetically "downhill" potential energy function for accommodation, steric barriers lead to highly-populated kinetic intermediates (Whitford et al., 2010a). Since these simulations displayed native-basin fluctuations that were consistent with anisotropic crystallographic analysis (Korostelev et al., 2008), explicit-solvent simulations, and normal mode calculations (Tama et al., 2003; Wang et al., 2004; Trylska et al., 2005), the coupling between the global fluctuations and the large-scale aa-tRNA movement into the ribosome could be characterized. Since these simulations exhibited similar tRNA-elbow movements as measured in sm-FRET (Geggier et al., 2010; Whitford et al., 2010a), reliable details of aa-tRNA acceptor arm accommodation and entry of the 3' CCA end into the PTC could be gleaned.

text, there are many possible "effective perturbations" to the energy landscape upon dehydration and formation of crystal contacts in a lattice (depicted as gold and blue lines). Here, the effective perturbation may include the effects of agents, such as the antibiotics paromomycin and kirromycin, used to "trap" a particular conformation of the system. Collectively, these effects are depicted as increasing the depth of the A/T basin by approximately 5-fold, though crystallization likely has far larger affects on the landscape. While the depth of the basin may be increased by such perturbations, and possibly shifted (dashed blue line), the system is still subject to energetic fluctuations arising from the surrounding environment. Fluctuations of this nature lead to structural fluctuations inside the crystal, which can be partially described by the B-factor. When the crystallizing conditions are sufficient to yield high-resolution scattering patterns, the energy basin is sharply defined and the distribution of the "trapped" ensemble becomes narrow enough for atomic resolution structure determination to be achieved. In such cases, the system is often referred to as a single "state". Nonetheless, the energy landscape framework necessarily applies and the system is simply a narrowly-defined ensemble, with reduced-amplitude motions.

While the ensemble nature of biological molecules has been rigorously demonstrated for proteins (Frauenfelder et al., 1979, 1991), where dynamics characterized as "forever kicking and screaming" have been noted (Weber 1975), this notion has only recently been exploited to study the motions inside ribosome

crystals (Korostelev and Noller, 2007; Korostelev et al., 2008). Since each atom is subject to a unique set of interactions, the motions about the "trapped" basin are anisotropically distributed, both in direction and magnitude (Garcia, 1992; Garcia et al., 1997). Here, an analysis of residual motions observed reveals that tRNA molecules fluctuate in the crystal lattice in directions consistent with the translocation reaction coordinate. These data support the notion that tRNAs remain in constant motion on the ribosome as suggested by single-molecule methods (Blanchard et al., 2004; Lee et al., 2007; Geggier et al., 2010; Whitford et al., 2010a) and that the effective perturbations of the crystal condition attenuate the overall magnitude of motions observed.

8. Energy landscapes and cryo-EM

Sample heterogeneity constitutes a major resolution-limiting factor for solving structures using single particle cryo-EM (Spahn and Penczek, 2009). However, with the development of multiparticle methods of image processing it is now possible to directly visualize instrinsic conformational heterogeneity within ribosomal complexes (Klaholz et al., 2004; Schuette et al., 2009; Agirrezabala et al., 2008; Julian et al., 2008). Consideration of the energy landscape during the "plunging" process suggests that the reconstructions determined by this approach actually reflect the ensemble nature of the system under investigation (Fig. 5 B). Prior to freezing the sample in vitreous ice (quenching), the molecules under investigation are distributed among an ensemble of states according to the nature of the energy landscape. During quenching, the system responds to the perturbation and the energy landscape deforms in a time-dependent fashion. The rate and magnitude of the changes in the energy landscape depend on both the entropy of each configuration in the system (Wales, 2004) as well as the contribution of energetic interactions in each conformation. These energetic interactions can also be altered, such as the degree of screening of electrostatic interactions, which depends on the temperature-dependent dielectric constant of the solution (Landau et al., 1984). If quenching is sufficiently rapid, such that the glass transition temperature, T_g (Williams et al., 1955), is reached faster than the overall reconfiguration time of the system, then the ensemble of frozen molecules closely approximates the Boltzmann distribution of states in the system prior to freezing.

After freezing and imaging, multiparticle data processing methods enable sorting of the particle images and result in not one, but a set of reconstructions. However, while each structure within the set of reconstructions is often referred to as a "state", it represents the average of an ensemble of configurations, centered about a particular energetic minimum. High conformational flexibility of parts of a ribosomal complex can explain why certain parts of the density map may appear fragmented or may only be observed at low contour levels. For example, in the A/T state of the ribosome trapped during the accommodation process using the antibiotic kirromycin (Villa et al., 2009; Schuette et al., 2009), the authors found that the switch 1 helix of EF-Tu, a key structural element involved in GTPase activation, was found in a disordered, dynamic state during the switch from the GTP form to the GDP form.

As recent landmark investigations of spontaneous reverse translocation have demonstrated (Fischer et al., 2010), the development of time-resolved cryo-EM techniques may be used to report on the *pmf* along a reaction coordinate. In the regime where over a million images can be obtained (Ratje et al., 2010), probability distributions can be calculated by projecting each image onto a distinct reaction coordinate. When one has thousands of counts per bin, the noise due to sampling should be on the order of $1/\sqrt{N} \approx 3\%$, assuming the uncertainty in the measured population scales as $\sqrt{N}$. Since the *pmf* is proportional to ln(P), an uncertainty in P by a factor of 1.03 corresponds to a difference in the *pmf* of $k_BT(\ln(1.03\mathrm{P}) - \ln(\mathrm{P})) = 0.03\ k_BT$. The major caveat with such a venture is that, while the statistical noise due to sampling may be low, the uncertainty in the projection onto the coordinate and the noise present in each image can lead to much larger effects (see Fig. 2). Similar to smFRET, characterizing the statistical properties of each of the reaction coordinate projections represents a substantial challenge towards using cryo-EM to reveal the fine details of the energy landscape.

9. Exploring energy landscapes through simulation

As petaflop supercomputing (i. e. 10^{15} calculations per second) can now be achieved, molecular dynamics simulations of the 70S (and, in principle, 80S) ribosome functions are now accessible (Sanbonmatsu et al., 2005, Whitford et al., 2010a). With continued

technical advances, as well as the development of new computational approaches, it is worthwhile to assess current computing practices and identify how each approach may shed light on the details of the energy landscape. Here, the general approaches, considerations and limitations in simulating ribosome functions are outlined in order for the reader to assess the field's directions and capabilities.

The first consideration in a simulation is to choose which force field (potential energy function) is appropriate for the questions of interest. In semi-empirical force fields, such as AMBER[6] (Pearlman et al., 1995), one uses a classical potential energy function, where interaction energies of the four nucleotides and twenty amino acids are calibrated to experimental quantities or to quantum calculations. These same energies are applied to any RNA or protein simulated and the system is immersed in a box of water molecules and excess ions. This approach often provides information about rapid (sub-microsecond) movement on the landscape. An alternative approach is to employ potential energy functions with pre-defined properties, such that the landscapes may be tested against ribosome experiments. Through iterative comparison with experiments, this second approach allows for much longer timescales (milliseconds) and can identify which properties of the ribosome's free energy landscape are most important in determining function.

The length of the simulation, the employed force field, and the process of interest must all be considered when determining what aspects of the landscape are being probed in each computational study. Here, we discuss recent simulations using semi-empirical force fields to illustrate how the timescale of each simulation allows for specific insights into the character of the landscape. Using enhanced sampled methods (Sanbonmatsu, 2006a; Vaiana and Sanbonmatsu, 2009; Garcia and Sanbonmatsu, 2000) thermodynamic convergence (i. e. calculated thermodynamic quantities do not change with additional sampling) of 16S decoding center dynamics with and without a ligand bound were achieved in 17,000 and 2,000 nanoseconds, respectively. These thermodynamic measurements showed that a stochastic gating mechanism of A1492/A1493 is likely a low-energy process, where there is a balance of motions of the A1492 and A1493 bases into and out of helix 44 during aminoglycoside recognition (Sanbonmatsu, 2006a). While simulations of the full 70S ribosome (~3 million atoms) are too expensive to measure thermodynamics directly, the relaxation time of local fluctuations in tRNA position were measured to be on timescales of ~10 ns (Whitford et al., 2010b; 205–301 ns per simulation), which characterizes how tRNAs diffuse across the landscape. Simulations of three-way junctions (Besseová et al., 2010; 30–100 ns per simulation) demonstrated that the landscapes local to the crystal configurations are not deep energetic basins. Rather, rapid local reconfigurations on the landscape allow for flexibility, which is likely relevant during translation. Similar simulations with the CHARMM forcefield[7] (Brooks et al., 1983) of the nascent TnaC peptide inside the 23S tunnel (Trabuco et al., 2010; 120 ns per simulation) suggest that the interactions formed on short timescales (tens of nanoseconds) contribute to the arrested conformation being a deep minimum on the energy landscape.

The second approach to simulating ribosome landscapes is to employ effective potential energy functions that reflect principles suggested by ribosome experiments and physical arguments. Agreement between the resulting dynamics and experiments partially validates the proposed energy landscape. By varying the parameters of the simulation, one can also characterize features of the process that are robust and features that should be sensitive to the specific environmental conditions. Since the features of the potential energy surface are explicitly defined, effective perturbations may be introduced to understand how the ribosome responds to changes in the cellular environment.

Using effective potentials, the idea that accommodation is a downhill potential energy process was tested through simulations (Whitford et al., 2010a). The classical conformation was defined as the minimum of the potential energy function. By construction, the starting (A/T) configuration is higher in potential energy, which is consistent with the notion of tRNA molecules acting as molecular springs (Frank et al., 2005) that must be properly aligned to enter the A site (Sanbonmatsu, 2006b). Fig. 5 C shows a schematic of the effective potential energy function used in that study. Since the configurational entropy is determined by the accessible phase space, and the potential energy was completely devoid of energetic roughness, kinetic intermediates were the result of changes in

6 It should be noted that, for nucleic acids, the AMBER forcefield is generally regarded (by the computational community) as the most well-developed potential for empirical simulations.

7 The vast majority of CHARMM development has focused on the parameterization of amino acids, and not nucleic acids.

configurational entropy during accommodation. Since the kinetic proofreading mechanism (Hopfield, 1974) requires barriers to be associated with the selection process, it was anticipated that entropic/steric barriers would exist and serve to reject non-cognate aa-tRNAs. While enthalpic interactions may drive the aa-tRNA into the ribosome, the simulation data suggested that the loss of configurational entropy resists accommodation. This entropic penalty resulted in reversible accommodation attempts and a multi-step accommodation process, much like what was observed through smFRET.

10. Future outlook

Understanding the mechanisms of translation control is expected to be a critical area of research in the coming decade. As the ribosome is the central component of the translation apparatus and an integration point for regulation, the implementation of quantitative tools to explore the molecular determinants of ribosome function in greater depth will be vital to this pursuit. The arsenal of structural, kinetic and computational methods already available for interrogating intrinsic conformational changes of the ribosome and their relationship to function, have provided important new insights for the road ahead. The energy landscape underpinning ribosome conformational events has been shown to be sensitive to buffer conditions, tRNA ligands, translation factors and antibiotic inhibitors that bind directly to ribosomal RNA. These early insights speak to the inherently metastable nature of the ribosome's architecture, foreshadowing the existence of substantial distinctions in the energetics of ribosome function across domains of life and the potential to understand gene-specific regulatory events at the molecular scale. Such events include nascent chain stalling, stop codon readthrough, frameshifting as well as other dynamic recoding processes (Gesteland and Atkins, 1996).

The impact of single-molecule, cryo-EM, and theoretical/computational methods to advance our understanding of the mechanism of protein synthesis remains nascent. The implementation of multicolor FRET experiments, integrated platforms for simultaneous force and FRET measurements, high-throughput strategies, as well as sorting algorithms to further explore heterogeneities in the ensemble of particles are certain to provide access to numerous, untold discoveries. Continued advancement of the energy landscape framework of ribosome function through simulation will help provide a rigorous connection to an all-atom, molecular view of the system. As simulations are extending to experimentally attainable timescales (milliseconds), atomic simulations of translation processes enable a direct integration of structural, computational and kinetic fields. Such efforts will yield trajectories of motion and testable hypothesis about specific trajectories of motion. Experimentally validated trajectories may ultimately provide unforeseen insights into the basic transl ation mechanism as well as evolutionary distinctions that may exist between the translation apparatus of each organism. Such insights are expected to enrich our knowledge and understanding of cellular and therapeutic strategies for translation control.

References

Agirrezabala X, Lei J, Brunelle JL, Ortiz-Meoz RF, Green R, Frank J (2008) Visualization of the hybrid state of tRNA binding promoted by spontaneous ratcheting of the ribosome. Mol Cell 32: 190–197

Besseová I, Réblová K, Leontis NB, Sponer J (2010) Molecular dynamics simulations sugg est that RNA three-way junctions can act as flexible RNA structural elements in the ribosome. Nuc Acid Res DOI:10 1093/nar/gkq414

Best RB and Hummer G (2010) Coordinate-dependent diffusion in protein folding. 107: 1088–1093

Blanchard SC, Gonzalez RL, Kim HD, Chu S, Puglisi JD (2004a) tRNA selection and kinetic proofreading in translation. Nat Struct Mol Bio 11: 1008–1014

Blanchard SC, Kim HD, Gonzalez RL Jr, Puglisi JD, Chu S (2004b) tRNA dynamics on the ribosome during translation. Proc Nat Acad Sci USA. 101: 12 893–12 898

Blanchard SC (2009) Single-molecule observations of ribosome function. Curr Op Struct Bio 19: 103–109

Brooks BR, Bruccoleri RE, Olafson BD, States DJ, Swaminathan S, Karplus M (1983) CHARMM: A program for macromolecular energy, minimization, and dynamics calculations. J Comp Chem 4: 187–217

Bryngelson JD and Wolynes PG (1989) Intermediates and barrier crossing in a random energy model (with applications to protein folding). J Phys Chem 93: 6902–6915

Cho SS, Levy Y, Wolynes PG (2006) P versus Q: structural reaction coordinates capture protein folding on smooth landscapes. Proc Nat Acad Sci USA 103: 586: 591

Cornish PV, Ermolenko DN, Noller HF, Ha T (2008) Spontaneous intersubunit rotation in single ribosomes. Mol Cell 30: 578–588

Cornish P, Ermolenko D, Staple D, Hoang L, Hickerson R, Noller H, Ha T (2009) Following movement of the L1 stalk between three functional states in single ribosomes. Proc Nat Acad Sci USA106: 2571–2576

Das P, Moll M, Stamati H, Kavraki LE, Clementi C (2006) Low-dimensional, free-energy landscapes of protein-folding reactions by nonlinear dimensionality reduction. Proc Nat Acad Sci USA 103: 9885–9890

Demeshkina N, Jenner L, Yusupova G, Yusupov M (2010) Interactions of the ribosome with mRNA and tRNA. Curr Op Struct

Bio 20: 325–332
Dorner S, Brunelle JL, Sharma D, Green R (2006) The hybrid state of tRNA binding is an authentic translation elongation intermediate. Nat Struct Mol Biol 13: 234–241
Dudko OK, Hummer G, Szabo A (2006) Intrinsic rates and activation free energies from single-molecule pulling experiments. Phys Rev Lett 96: 108 101
Faradjian AK and Elber R (2004) Computing time scales from reaction coordinates by milestoning. J Chem Phys 120: 10 880–10 889
Fei J, Kosuri P, MacDougall DD, Gonzalez RL Jr. (2008) Coupling of ribosomal L1 stalk and tRNA dynamics during translation elongation. Mol Cell 30: 348–359
Fei J, Bronson JE, Hofman JM, Srinivas RL, Wiggins CH, Gonzalez RL (2009) Allosteric collaboration between elongation factor G and the ribosomal L1 stalk directs tRNA movement during translation. Proc Nat Acad Sci USA 106: 15 702–15 707
Fischer N, Konevega AL, Wintermeyer W, Rodnina MV, Stark H (2010) Ribosome dynamics and tRNA movement by time-resolved electron cryomicroscopy. Nature 466: 329–333
Fluitt A, Pienaar E, Viljoen H (2007) Ribosome kinetics and aa-tRNA competition determine rate and fidelity of peptide synthesis. Comp Bio Chem 31: 335–346
Frank J, Sengupta J, Gao H, Li W, Valle M, Zavialov A, Ehrenberg M (2005) The role of tRNA as a molecular spring in decoding, accommodation, and peptidyl transfer. FEBS Lett 579: 959–962
Frank J, Spahn CM (2006) The ribosome and the mechanism of protein synthesis. Rep Prog Phys 69: 1383–1417
Frank J, Gao H, Sengupta J, Gao N, Taylor DJ (2007) The process of mRNA-tRNA translocation. Proc Nat Acad Sci USA 104: 19 671–19 678
Frauenfelder H, Petsko GA, Tsernoglou D (1979) Temperature-dependent x-ray-diffraction as a probe of protein structural dynamics. Nature 280: 558–563
Frauenfelder H, Sligar SG, Wolynes PG (1991) The energy landscapes of motions of proteins. Science 254: 1598–1603
Gao Y-G, Selmer M, Dunham CM, Weixlbaumer A, Kelley AC, Ramakrishnan V (2009) The structure of the ribosome with elongation factor G trapped in the posttranslocational state. Science 326: 694–699
Garcia AE (1992) Large-amplitude nonlinear motions in proteins. Phys Rev Lett 68: 2696–2699
Garcia AE and Onuchic JN (2003) Folding a protein in a computer: An atomic description of the folding/unfolding of protein A. Proc Nat Acad Sci USA 13 898–13 903
Garcia AE, Krumhansl JA, Frauenfelder H (1997) Variations on a theme by Debye and Waller: From simple crystals to proteins. Prot Struct Func Gen 29: 153–160
Gavrilova LP, Kostiashkina OE, Koteliansky VE, Rutkevitch NM, Spirin AS (1976) Factor-free ("non-enzymic") and factor-dependent systems of translation of polyuridylic acid by Escherichia coli ribosomes. J Mol Biol 101: 537–552
Geggier P, Dave R, Feldman MB, Terry DS, Altman RB, Munro JB, Blanchard SC (2010) Conformational sampling of aminoacyl-tRNA during selection on the ribosome. J Mol Biol doi:10 1016/j. jmb.2010.04 038
Gesteland RF, Atkins JF (1996) Recoding: dynamic reprogramming of translation. Annu Rev Biochem 65: 741–68
Gromadski KB and Rodnina MV (2004) Kinetic determinants of high-fidelity tRNA discrimination on the ribosome. Mol Cell 13: 191–200
Hyeon C and Onuchic JN (2007) Mechanical control of the directional stepping dynamics of the kinesin motor. Proc Nat Acad Sci USA 104: 17 382–17 387
Hopfield JJ (1974) Kinetic proofreading: A new mechanism for reducing errors in biosynthetic processes requiring high specificity. Proc Nat Acad Sci USA 71: 4135–4139
Johansson M, Bouakaz E, Lovmar M, Ehrenberg M (2008) The kinetics of ribosomal peptidyl transfer revisited. Mol Cell 30: 589–598
Julian P, Konevega AL, Scheres SH, Lazaro M, Gil D, Wintermeyer W, Rodnina MV, Valle M (2008) Structure of ratcheted ribosomes with tRNAs in hybrid states. Proc Nat Acad Sci USA 105: 16 924–16 927
Klaholz BP, Myasnikov AG, van Heel M (2004) Visualization of release factor 3 on the ribosome during termination of protein synthesis. Nature 427: 862–865
Klepeis JL, Lindorff-Larsen K, Dror RO, Shaw DE (2009) Long-timescale molecular dynamics simulations of protein structure and function. Curr Opin Struct Biol 19: 120–127
Komatsuzuki T, Hoshino K, Matsunaga Y, Rylance GJ, Johnston RL, Wales DJ (2005) How many dimensions are required to approximate the potential energy landscape of a model protein? J Chem Phys 122: 084 714
Korostelev A and Noller HF (2007) Analysis of structural dynamics in the ribosome byTLS crystallographic refinement. J Mol Biol 373: 1058–1070
Korostelev A, Asahara H, Lancaster L, Laurberg M, Hirschi A, Zhu J, Trakhanov S, Scott WG, Noller HF (2008) Crystal structure of a translation termination complex formed with release factor RF2. Proc Nat Acad Sci USA 105: 19 684–19 689
Landau LD, Lifshitz EM, Pitaevskii LP (1984) Electrodynamics of continuous media (2nd ed.) Reed educational and professional publishing, Oxford, England
Lee T-H, Blanchard SC, Kim HD, Puglisi JD, Chu S (2007) The role of fluctuations in tRNA selection by the ribosome. Proc Nat Acad Sci USA 104: 13 661–13 665
Leopold PE, Montal M, Onuchic JN (1992) Protein folding funnels-A kinetic approach to the sequence structure relationship. Proc Nat Acad Sci USA 89: 8721–8725
Lu Q and Wang J (2009) Kinetics and statistical distributions of single-molecule conformational dynamics. J Phys Chem B 113: 1517–1521
Marshall RA, Dorywalska M, Puglisi JD (2008) Irreversible chemical steps control intersubunit dynamics during translation. Proc Nat Acad Sci USA 105: 15 364–15 369
Miyashita O, Onuchic JN, Wolynes PG (2003) Nonlinear elasticity, proteinquakes, and the energy landscapes of functional transitions in proteins. Proc Nat Acad Sci USA 100: 12 570–12 575
Munro JB, Altman RB, O'Connor, Blanchard SC (2007) Identification of two distinct hybrid-state intermediates on the ribosome. Mol Cell 25: 505–517
Munro JB, Sanbonmatsu KY, Spahn CMT, Blanchard SC (2009) Navigating the ribosome's metastable energy landscape. Trends Biochem Sci 34: 390–400
Munro JB, Altman RB, Tung C-S, Sanbonmatsu KY, Blanchard SC (2010a) A fast dynamic mode of EF-G-bound ribosome. EMBO J 29: 770–781
Munro JB, Altman RB, Tung C-S, Cate JDH, Sanbonmatsu KY, Blanchard SC (2010b) Spontaneous formation of the unlocked state of the ribosome is a multistep process. Proc Nat Acad Sci USA 107: 709–714
Nettels D, Gopich IV, Hoffman A, Schuler B (2007) Ultrafast dynamics of protein collapse from single-molecule photon statistics. Proc Nat Acad Sci USA 104: 2655–2660
Nettels D, Hoffmann A, Schuler B (2008) Unfolded protein and peptide dynamics investigated with single-molecule FRET and correlation spectroscopy from picoseconds to seconds.

J Phys Chem B 112: 6137–6146
Nymeyer H, Socci ND, Onuchic JN (2000) Landscape approaches for determining the ensemble of folding transition states: Success and failures hinge on the degree of frustration. Proc Nat Acad Sci USA 97: 634–639
Oliveira RJ, Whitford PC, Chahine J, Wang J, Onuchic JN, Leite VBP (2010) Exploring the origin of non-monotonic complex behavior and the effects of non-native interactions on the diffusive properties of protein folding. Biophys J In Press
Onuchic JN, Wolynes PG (1993) Energy landscapes, glass transitions, and chemical reaction dynamics in biomolecular or solvent environment. J Chem Phys 98: 2218–2224
Onuchic JN, Nymeyer H, Garcia AE, Chahine J, Socci ND (2000) The energy landscape theory of protein folding: Insights into folding mechanisms and scenarios. Adv Protein Chem 53: 87–152
Onuchic JN, Kobayashi C, Miyashita O, Jennings P, Baldridge KK (2006) Exploring biomolecular machines: energy landscape control of biological reactions. Philos Trans Royal Soc 361: 1439–1443
Orzechowski M and Tama F (2008) Flexible fitting of high-resolution X-ray structures into cryo-electron microscopy maps using biased molecular dynamics simulations. Biophys J 95: 5692–5705
Pape T, Wintermeyer W, Rodnina M (1999) Induced fit in initial selection and proofreading of aminoacyl-tRNA on the ribosome. EMBO J 18: 3800–3807
Pearlman DA, Case DA, Caldwell JW, Ross WS, Cheatham TE III, DeBolt S, Ferguson D, Seibel G, Kollman P (1995) AMBER, a package of computer programs for applying molecular mechanics, normal mode analysis, molecular dynamics and free energy calculations to simulate the structural and energetic properties of molecules. Comp Phys Commun 91: 1–41
Penczek PA, Frank J, Spahn CMT (2006) A method of focused classification, based on the bootstrap 3D variance analysis, and its applications to EF-G-dependent translocation. 154: 184–194
Peng C, Zhang L, Head-Gordon T (2010) Instantaneous normal modes as an unforced reaction coordinate for protein conformational transitions. Biophys J 98: 2356–2364
Pérez A, Marchán I, Svozil D, Sponer J, Cheatham TE III, Laughton CA, Orozco M (2007) Refinement of the AMBER force field for nucleic acids: Improving the description of α/(conformers. Biophys J 92: 3817–3829
Pincus DL, Cho SS, Hyeon C, Thirumalai D (2009) Minimal models for proteins and RNA: From folding to function. In: Molecular Biology of protein folding, Vol 84, pp. 203–250. Elsevier Academic, San Diego, CA
Ratje AH, Loerke J, Mikolajka A, Brünner M, Hildebrand PW, Starosta A, Doenhoefer A, Connel SR, Fucini P, Mielke T, Whitford PC, Onuchic JN, Yu Y, Sanbonmatsu KY, Hartmann RK, Penczek PA, Wilson DN, Spahn CMT (2010) Head swivel on the ribosome facilitates translocation via intra-subunit tRNA hybrid sites. Under Review
Roberts E, Sethi A, Montoya J, Woese CR, Luthey-Schulten Z (2008) Molecular signatures of ribosomal evolution. Proc Nat Acad Sci USA 105: 13 953–13 958
Roberts RW, Eargle J, Luthey-Schulten Z (2010) Experimental and computational determination of tRNA dynamics. FEBS Lett 584: 376–386
Rodnina MV and Wintermeyer W (2001) Fidelity of aminoacyl-tRNA selection on the ribosome: Kinetic and structural mechanisms. Annu Rev Biochem 70: 415–435
Sanbonmatsu KY (2006a) Energy landscape of the ribosomal decoding center. Biochimie 88: 1053–1059
Sanbonmatsu KY (2006b) Alignment/misalignment hypothesis for tRNA selection by the ribosome. Biochimie 88: 1075–1089
Sanbonmatsu KY and Tung C-S (2007) High performance computing in biology: Multimillion atom simulations of nanoscale systems. J Struct Bio 157: 470–480
Schmeing TM, Voorhees RM, Kelley AC, Gao Y-G, Murphy FV, Weir JR, Ramakrishnan V (2009) The crystal structure of the ribosome bound to EF-Tu and aminoacyl-tRNA. Science 326: 688–694
Schuette J-C, Murphy FC, Kelly AC, Weir JR, Geisebrecht J, Connell SR, Loerke J, Mielke T, Zhang W, Penczek PA, Ramakrishnan V, Spahn CMT (2009) GTPase activation of elongation factor EF-Tu by the ribosome during decoding. EMBO 28: 1–11
Schuler B, Lipman EA, Eaton WA (2002) Probing the free-energy surface for protein folding with single-molecule fluorescence spectroscopy. Nature 419: 743–748
Sievers A, Beringer M, Rodnina MV, Wolfenden R (2004) The ribosome as an entropy trap. Proc Nat Acad Sci USA 101: 7897–7901
Spahn CMT, Penczek PA (2009) Exploring conformational modes of macromolecular assemblies by multiparticle cryo-EM. Curr Opin Struct Biol 19: 623–631
Spirin AS (2009) The ribosome as a conveying thermal ratchet machine. J Biol Chem 284: 21 103–21 119
Stanley RE, Blaha G, Grodzicki RL, Strickler MD, Steitz TA (2010) The structures of the anti-tuberculosis antibiotics viomycin and capreomycin bound to the 70S ribosome. Nat Struct Mol Biol 17: 289–293
Tama F, Valle M, Frank J, Brooks CL III (2003) Dynamic reorganization of the functionally active ribosome explored by normal mode analysis and cryo-electron microscopy. Proc Nat Acad Sci USA 100: 9319–9323
Tang J, Kang S-G, Saven, JG, Gai F (2009) Characterization of the cofactor-induced folding mechanism of a zinc-binding peptide using computationally designed mutants. J Mol Biol 389: 90–102
Trabuco LG, Harrison CB, Schreiner E, Schulten K (2010) Recognition of the regulatory nascent chain TnaC by the ribosome. Structure 18: 627–637
Thirumalai D and Hyeon C (2005) RNA and protein folding: Common themes and variations. Biochem 44: 4957–4970
Thirumalai D, O'Brien EP, Morrison G, Hyeon C (2010) Theoretical perspectives on protein folding. Annu Rev Biophys 39: 159–183
Trylska J, Tozzini V, McCammon JA (2005) Exploring global motions and correlations in the ribosome. Biophys J 89: 1455–1463
Vaiana AC and Sanbonmatsu KY (2009) Stochastic gating and drug-ribosome interactions. J Mol Biol 386: 648–661
Vanheel M and Frank J (1981) Use of multivariate statistics in analyzing the images of biological macromolecules. Ultramicroscopy 6: 187–194
Villa E, Sengupta J, Trabuco L, LeBarron J, Baxter WT, Shaikh TR, Grassucci RA, Nissen P, Ehrenberg M, Schulten K, Frank J (2009) Ribosome-induced changes in elongation factor Tu conformation control GTP hydrolysis. Proc Nat Acad Sci USA 106: 1063–1068
Wales DJ (1984) Energy Landscapes: Applications to clusters, biomolecules and glasses. Cambridge University Press, Cambridge, England
Wang J (2003) Statistics, pathways and dynamics of single molecule protein folding. J Chem Phys 118: 952–958
Wang Y, Rader AJ, Bahar I, Jernigan RL (2004) Global ribosome motions revealed with elastic network model. J Struct Biol

147: 302–314
Weber G (1975) Energetics of ligand binding to proteins. Adv Protein Chem 29: 1–83
Wekselmen I, Davidovich C, Agmon I, Zimmerman E, Rozenberg H, Bashan A, Birisio R, Yonath A. (2009) Ribosome's mode of function: myths, facts and recent results. J Pept Sci 15: 122–130
Whitford PC, Miyashita O, Levy Y, Onuchic JN (2007) Conformational transistions of adenylate kinase: switching by cracking. J Mol Biol 366: 1661–1671
Whitford PC, Noel JK, Gosavi S, Schug A, Sanbonmatsu KY, Onuchic JN (2009a) An all-atom structure-based potential for proteins: Bridging minimal models with all-atom empirical forcefields. Prot Struc Func Bioinfo 75: 430–441
Whitford PC, Schug A, Saunders J, Hennelly SP, Onuchic JN, Sanbonmatsu KY (2009b) Nonlocal helix formation is key to understanding S-Adenosylmethionine-1 riboswitch function. Biophys J 96:L7-L9
Whitford PC, Geggier P, Altman RB, Blanchard SC, Onuchic JN, Sanbonmatsu KY (2010a) Accommodation of aminoacyl-tRNA into the ribosome involves reversible excursions along multiple pathways. RNA DOI: 10 1261/rna.2 035 410
Whitford PC, Onuchic JN, Sanbonmatsu KY (2010b) Connecting energy landscapes with experimental rates for aminoacyl-tRNA accommodation in the ribosome *(submitted)*
Williams ML, Landel RF, Ferry JD (1955) Mechanical properties of substances of high molecular weight. 19. The temperature dependence of relaxation mechanisms in amorphous polymers and other glass-forming liquids. J Amer Chem Soc 77: 3701–3707
Wong V and Case DA (2008) Evaluating rotational diffusion from protein MD simulations. J Phys Chem B 112: 6013–6024. Yang S and Roux B (2008) Src kinase conformational activation: Thermodynamics, pathways, and mechanisms. Plos Comp Biol doi: 0.1371/journal. pcbi.10 00 047
Yusupov MM, Yusupova GZ, Baucom A, Leiberman K, Earnest TN, Cate JH, Noller HF (2001) Crystal structure of the ribosome at 5.5 Å. Science 292: 883–896
Zhang G, Feyunin I, Miekley O, Valleriani A, Moura A, Ignatova Z (2010) Global and local depletion of ternary complex limits translation elongation. Nuc Acid Res doi:10 1093/nar/gkq196
Zhang W, Dunkle A, Cate JHD (2009) Structures of the ribosome in intermediate states of ratcheting. Science 325: 1014–1017
Zwanzig R (1988) Diffusion in a rough potential. Proc Nat Acad Sci USA 85: 2029–2030